COMPUTER-AIDED CIVIL AND INFRASTRUCTURE ENGINEERING

Computer-Aided Civil and Infrastructure Engineering **33** (2018) 411–422

A Quantum-Inspired Genetic Algorithm-Based Optimization Method for Mobile Impact Test Data Integration

Wenju Zhao & Shuanglin Guo

Jiangsu Key Laboratory of Engineering Mechanics, Southeast University, Nanjing, China

Yun Zhou

College of Civil Engineering, Hunan University, Changsha, China

&

Jian Zhang*

Jiangsu Key Laboratory of Engineering Mechanics, Southeast University, Nanjing, China

Abstract: *The traditional impact test method needs a large number of sensors deployed on the entire structure, which cannot meet the requirements of rapid bridge testing. A new mobile impact test method is proposed by sequentially testing the substructures then integrating the test data of all substructures for flexibility identification of the entire structure. The novelty of the proposed method is that the quantum-inspired genetic algorithm (QIGA) is proposed to improve computational efficiency by transforming the scaling factor sign determination problem to an optimization problem. Experimental example of a steel–concrete composite slab and numerical example of a three-span continuous rigid-frame bridge are studied which successfully verify the effectiveness of the proposed method.*

1 INTRODUCTION

Structural health monitoring (SHM) technology has been widely utilized to identify structural characteristics, and locate and quantify structural damages (Li et al., 2006; Catbas et al., 2013; Amezquita-Sanchez and Adeli, 2014). As a widely used solution for SHM, ambient vibration testing, which adopts traffic flows and wind loads etc. to be the natural excitation sources, has been applied in many long-span bridges, such as the Vincent Thomas Bridge (He et al., 2008), the Humber Bridge (Brownjohn et al., 2010), and the Throgs Neck Bridge (Zhang et al., 2013a). Besides, with the finite element (FE) model-driven approach, ambient vibration test data can be used to identify more detailed structural parameters. However, how to decide the single dominant model from many models with high plausibility and uncertainty is still another vital problem (Zhang et al., 2013b).

Multiple reference impact testing (MRIT) used a hammer or other exciters to impact the bridge's deck, during which the impact force and the structural response under the force are recorded for structural identification (Brown and Witter, 2011). Catbas et al. (2004) developed the complex mode indicator function (CMIF) algorithm to process the impact test data and applied it to an aged highway bridge. De Vitis et al. (2013) proposed an impacting device for rapid structural identification of highway bridges. Zhang et al. (2014) proved that the impact test method with collecting force data has the advantage of identifying the magnitudes of structural frequency response functions

*To whom correspondence should be addressed. E-mail: *Jianzhang.civil@gmail.com*.

[Correction added on April 11, 2018, after first online publication: order of authors updated]

DOI: 10.1111/mice.12352

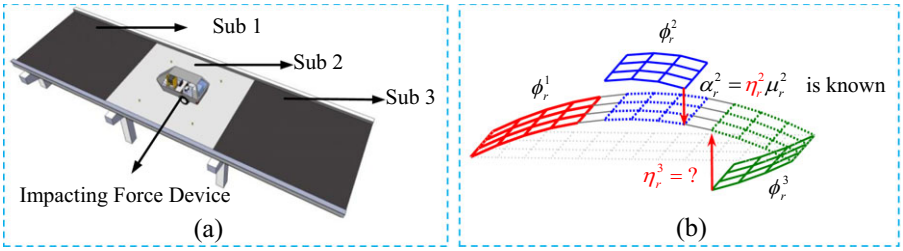

Fig. 1. Mobile impact testing with reference-free measurement: (a) the framework of the method and (b) the problem of the method.

(FRFs), and which are necessary for structural flexibility identification. However, the limitation of the traditional impact test method lies in that it requires a large number of sensors deployed on the entire structure, which usually leads to expensive experimental costs. To overcome the limitation, the idea of mobile impact testing emerges naturally by dividing a structure into substructures then sequentially performing the impact test on substructures. Subsequently, the emerging problem is how to integrate the test data of substructures for modal identification of the entire structure. Although there are many decentralized modal identification algorithms processing the ambient vibration data (Lynch, 2002; Sadhu et al., 2014; Marulanda et al., 2016), they cannot be transplanted directly to solve the data integration problem of the mobile impact test method. To address the above challenging problem, Zhang et al. (2015) developed the interface measurement-based approach and the single reference-based approach to integrate all substructures' vibration data for identifying the entire structure's flexibility matrix. The method of mobile impact test with single-reference measurement (Figure 1) not only increases one more sensor, but also requires the extra labor to acquire the response of the single reference node repetitively in all impact tests of substructures especially when the reference node is far away.

To achieve the purpose of rapid impact testing for bridges, a mobile impact test method with reference-free measurement is proposed by Zhang et al. (Guo et al., 2018). As shown in Figure 1a, the structure is divided into three substructures and the impact test is independently conducted on each substructure one by one. The FRFs of three substructures ($\mathbf{H}^{11}$, $\mathbf{H}^{22}$, and $\mathbf{H}^{33}$) are estimated respectively using the recorded input forces and accelerations, from which basic modal parameters (system poles (λ_r^1, λ_r^2, and λ_r^3), modal scaling factors (Q_r^1, Q_r^2, and Q_r^3), mode shapes (ψ_r^1, ψ_r^2, and ψ_r^3), and modal participation factors (Γ_r^1, Γ_r^2, and Γ_r^3) of three substructures and their modal flexibility matrices ($\mathbf{f}_r^1$, $\mathbf{f}_r^2$, and $\mathbf{f}_r^3$) are identified respectively. However, because impact testing of each substructure is independent, the scaling factors of the substructure mode shapes in some mode are not at a same scaling level. It is shown that the sign factors, η_r^k, are still unknown so far though they are either 1 or –1, which means that the orientation of each substructure's scaled mode shape has not yet been determined. This phenomenon is shown in Sub 3 in Figure 1b. Therefore, a method based on the principle of minimum potential energy (PMPE) was proposed to determine the signs by sorting all possible cases of potential energy (PE) and finding the minimum one.

However, it is obvious that the computation efficiency will be very low if enumerating all values of PE when the scale of the question becomes large. Also, due to the noise involved in the measurement, multiple local minimum values even the ill-conditioned minimum that do not obey the continuity or basic physical laws will happen when the searching process of the sign factors is carried out. To optimally improve the testing efficiency and acquire the higher mode information, the question of assembling substructures' mode shapes into the global mode shapes of the entire structure is transformed into an optimization problem in this article, which falls into the NP-hard binary optimization paradigm. Thus, swarm and evolutionary computations based algorithms to solve the optimization problem are required. There are abundant applications of swarm and evolutionary computations in civil engineering, such as Genetic Algorithm (Han and Kim, 2000; Jiang and Adeli, 2008; Sgambi et al., 2012; Kociecki and Adeli, 2014; Cha and Buyukozturk, 2015; Mencia et al., 2016), Ant Colony Algorithm (Putha et al., 2012), and Particle Swarm Optimization (Shabbir and Omenzetter, 2015). In this article, an improved quantum-inspired genetic algorithm (QIGA) is developed because of its excellent performance.

The structure of the article is as follows: in Section 2, the framework of the improved QIGA with dynamic quantum rotation gate and adaptive crossover (mutation) probability rate is developed to solve the scaling factor sign determination problem. In Sections 3 and 4, the experimental example of a steel–concrete composite slab and the numerical example of a three-span

continuous rigid-frame bridge are studied respectively to verify the effectiveness of the proposed method. Finally, conclusions are drawn.

2 FRAMEWORK OF THE QIGA-BASED ALGORITHM METHOD FOR SOLVING THE OPTIMIZATION PROBLEM

As shown in Figure 2, the strategy of the traditional method is sorting all possible cases of potential energy and finding the minimum one, which means that the computation efficiency will be very low when the case number becomes large. Therefore, a modified QIGA is developed to solve the optimization problem.

The QIGA is a probabilistic evolutionary algorithm that embeds the quantum computation into the classical genetic algorithm (GA). The hybrid strategy enables this algorithm not only to share with some common operations like crossover and mutation in classical GA, but also to have quantum characteristics such as quantum rotation gate and measurement of collapse. In QIGA, the basic unit is the quantum bit (Q-bit). It is usually expressed with $[\alpha \quad \beta]^T$ or the Bra-Ket notation $|\psi\rangle = \alpha|0\rangle + \beta|1\rangle$, in which α^2 and β^2 are the probability of appearing in the state 0 and the state 1 respectively and they follow the principle of unit normalization $\alpha^2 + \beta^2 = 1$. The position represented by a Q-bit may locate in the state 0, the state 1, or in a linear superposition of both, which is different from classical state. The state transition can be achieved by quantum rotation gate that is defined as follows:

$$\begin{aligned}\mathbf{U}(\Delta\theta) &= \begin{bmatrix} \cos(\Delta\theta) & -\sin(\Delta\theta) \\ \sin(\Delta\theta) & \cos(\Delta\theta) \end{bmatrix}, \begin{bmatrix} \alpha' \\ \beta' \end{bmatrix} \\ &= \mathbf{U}(\Delta\theta) \begin{bmatrix} \alpha \\ \beta \end{bmatrix} \end{aligned} \tag{1}$$

where $[\alpha' \quad \beta']^T$ is the Q-bit after updating; $\mathbf{U}(\Delta\theta)$ is the rotation gate and correspondingly $\Delta\theta$ is the rotation angle, whose two attributes, size and sign, are usually determined by an adjustment strategy designed in advance (Han and Kim, 2000).

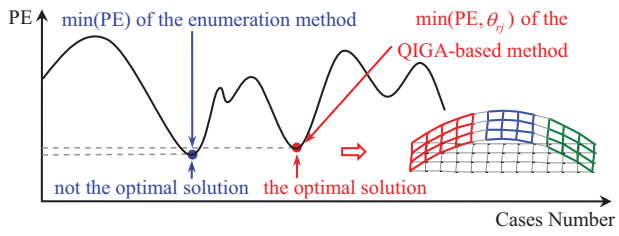

Fig. 2. Overview of the proposed method.

For the specific optimization problem studied in this article, the first focus is to design the encoding scheme for its variables, the undetermined sign factors, to solve them using QIGA. Owing to the number of substructures and mode orders are m and N respectively, so there are $N(m-1)$ sign factors. Therefore, the length of the encoded quantum chromosome is $N(m-1)$. The matrix form of the sign factors η_r is not suitable for encoding, and hence they are rearranged as the following row vector:

$$\left[\underbrace{\eta_1^1 \cdots \eta_1^{m-1}}_{r=1} \quad \cdots \quad \underbrace{\eta_r^1 \cdots \eta_r^{m-1}}_{r=r} \quad \cdots \quad \underbrace{\eta_N^1 \cdots \eta_N^{m-1}}_{r=N} \right] \tag{2}$$

Correspondingly, the encoding for the quantum chromosome should have the same sequence as following:

$$\left[\begin{matrix} \alpha_1^1 \cdots \alpha_1^{m-1} \\ \underbrace{\beta_1^1 \cdots \beta_1^{m-1}}_{r=1} \end{matrix} \cdots \begin{matrix} \alpha_r^1 \cdots \alpha_r^{m-1} \\ \underbrace{\beta_r^1 \cdots \beta_r^{m-1}}_{r=r} \end{matrix} \cdots \begin{matrix} \alpha_N^1 \cdots \alpha_N^{m-1} \\ \underbrace{\beta_N^1 \cdots \beta_N^{m-1}}_{r=N} \end{matrix} \right] \tag{3}$$

From Equations (2) and (3), the single Q-bit $[\alpha_r^k \quad \beta_r^k]^T$ represents the state of sign factor η_r^k, in which $(\alpha_r^k)^2$ specifies the probability of $\eta_r^k = 1$ and $(\beta_r^k)^2$ specifies the probability of $\eta_r^k = -1$. Adopting this encoding scheme for the optimization problem, the quantum chromosome can be updated by using classical evolutionary operators such as crossover and mutation as well as the quantum rotation gate applied on the single Q-bit. Thus, the whole population can rapidly evolve with cyclic iterations.

It is worth mentioning that important parameters including the rotation angle, the probabilities of crossover and mutation greatly influence the performance of the QIGA. To improve the computational efficiency of the optimization problem, the following works are how to design the dynamic rotation angle, the adaptive crossover and mutation probabilities.

2.1 The dynamic quantum rotation gate

For conventional genetic quantum algorithm, the rotation angle $\Delta\theta$ is a constant, which reduces the possibility to escape from local optima. To overcome this shortcoming, a dynamic rotation angle is designed according to the pattern shown in Figure 3.

It can be seen that this strategy of dynamic rotation angle is able to change dynamically with the fitness of the individuals. Mathematically, if an individual's encoding is far away from the best one, a relative large rotation angle will work to search the optima for the objective function at a large stride on the whole search region. By contrast, when an individual's encoding

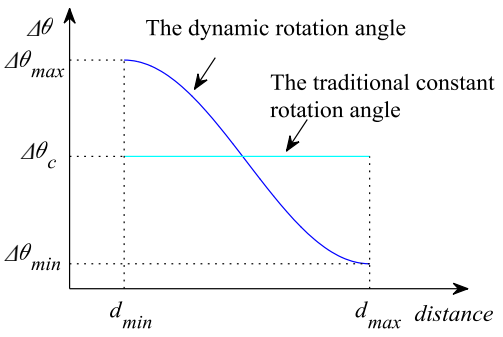

Fig. 3. The dynamic rotation angle line.

approaches to the best one, a relative small rotation angle is needed to carefully search the local optimal region. The following specific formula just matches with the strategy of the proposed dynamic rotation angle.

$$\Delta\theta_i = a + b \times \sin(c + e \times d_i) \tag{4}$$

where $a = \frac{\Delta\theta_{max}+\Delta\theta_{min}}{2}$, $b = -\frac{\Delta\theta_{max}-\Delta\theta_{min}}{2}$ and $c = -\frac{\pi}{2}\frac{(d_{max}+d_{min})}{(d_{max}-d_{min})}$ and $e = \frac{\pi}{d_{max}-d_{min}}$; $\Delta\theta_{max}$ and $\Delta\theta_{min}$ are the upper and the lower limits of the dynamic quantum rotation angle, respectively. In this article, $\Delta\theta_{max} = 0.05\pi$ and $\Delta\theta_{min} = 0.001\pi$ are used; $d_i = 1 - h_i/L$, where h_i is the Hamming distance between the genes of the individual and the genes of the best one; that is to say, the number of different values between two binary strings at the same bit. L is the length of the individual chromosome. d_{max} and d_{min} are the maximum and the minimum values among all d_i, respectively.

2.2 The adaptive crossover (mutation) strategy

Although there are some methods to design the adaptive crossover and mutation probabilities (Beg and Islam, 2016), the difference between the traditional and the proposed strategy are illustrated in Figure 4.

It can be clearly seen that the proposed adaptive operators in this article are not only in response to the fitness values of the solutions adaptively, but also have the exponential smooth transition properties. The adaptive crossover strategy (Figure 4a) can provide the possibility of the diversity of the population during the individual approaches to the best individual in the population. Also the adaptive mutation strategy (Figure 4b) can provide the possibility to jump out of the local optimum such that the population can evolve to a better state. The proposed adaptive crossover strategy is defined as

$$p_{c,i} = \begin{cases} p_{c,\max}, & f_i < f_{\text{mean}} \\ p_{c,\max} - \dfrac{p_{c,\max} - p_{c,\min}}{\tanh(\rho)} \times \tanh\left(\dfrac{\rho(f_i - f_{\text{mean}})}{f_{\max} - f_{\text{mean}}}\right), & f_i \geq f_{\text{mean}} \end{cases} \tag{5}$$

where $p_{c,\max}$ and $p_{c,\min}$ are the upper and the lower limits of the crossover probability respectively, $p_{c,\max} = 0.9$ and $p_{c,\min} = 0.5$ are used in this article; f_i, f_{mean} and $f_{\max}$ are the fitness value of the population respectively; $\tanh(\cdot)$ is the Hyperbolic Tangent Function ($\tanh(x) = \frac{e^x - e^{-x}}{e^x + e^{-x}}$), $\rho(\rho > 0)$ is an accelerating factor to regulate the evolution speed of the population, and $\rho = 5$ is used in this article. It should be noted that a too large value of ρ is prohibited because it may cause the population to evolve in a local optima prematurely. The proposed adaptive mutation strategy is given as

$$p_{m,i} = \begin{cases} p_{m,\max}, & f_i < f_{\text{mean}} \\ p_{m,\min} + \dfrac{p_{m,\max} - p_{m,\min}}{\tanh(\rho)} \times \tanh\left(\dfrac{\rho(f_{\max} - f_i)}{f_{\max} - f_{\text{mean}}}\right), & f_i \geq f_{\text{mean}} \end{cases} \tag{6}$$

where $p_{m,\max}$ and $p_{m,\min}$ are the upper and the lower limits of the mutation probability respectively, $p_{m,\max} = 0.2$ and $p_{m,\min} = 0.01$ are used in this article. The factor

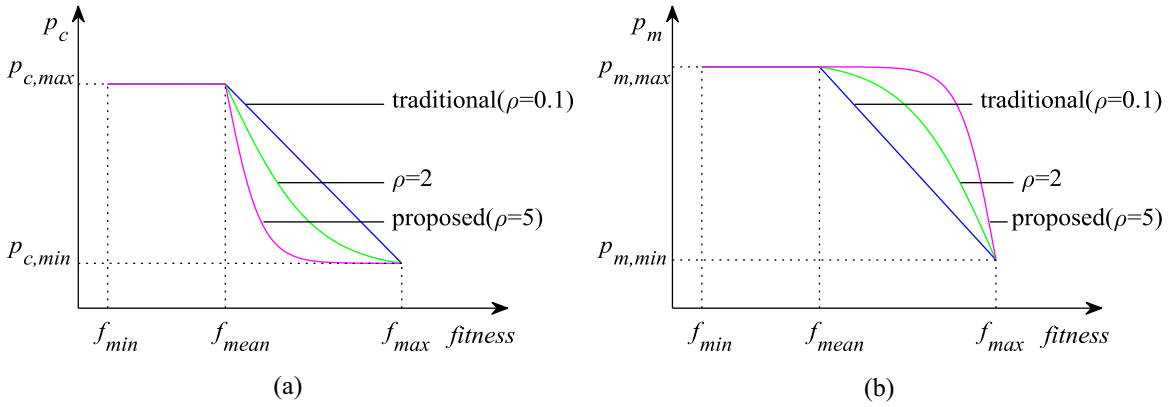

Fig. 4. The variation operators with different bending parameter ρ: (a) the crossover strategy and (b) the mutation strategy.

ρ in Equation (6) has the same meaning and value as it is in Equation (5).

2.3 The fitness function

It is well known that the accurate displacement of a structure induced by static forces will minimize the structure's potential energy, which can be calculated by,

$$\pi_p(\eta_r) = \frac{1}{2}\sum_{r=1}^{N}\left[(\mathbf{F}^T\mathbf{T}_r\eta_r\nu_r\psi_r)^2\left(\frac{Q_r^{\text{master}}}{\lambda_r^{\text{master}}}+\frac{Q_r^{\text{master}*}}{\lambda_r^{\text{master}*}}\right)\right] \tag{7}$$

where $\mathbf{F}^T=\{\mathbf{F}^{1T}\ \cdots\ \mathbf{F}^{mT}\}^T\in\mathbb{R}^{N_0\times 1}$ is the static force vector applied on each output node of the entire structure and correspondingly; $\mathbf{F}^m\in\mathbb{R}^{N_0^m\times 1}$ is the one applied on the mth substructure; $\psi_r\in\mathbb{C}^{N_0\times 1}$ is the rth inconsistent mode shape of the entire structure; $\mathbf{T}_r=\eta_r\nu_r=\begin{bmatrix}\nu_r^1\mathbf{I}_{N_0^1} & & \\ & \ddots & \\ & & \nu_r^m\mathbf{I}_{N_0^m}\end{bmatrix}\begin{bmatrix}\eta_r^1\mathbf{I}_{N_0^1} & & \\ & \ddots & \\ & & \eta_r^m\mathbf{I}_{N_0^m}\end{bmatrix}$ is the transfer matrix, where $\mathbf{I}_{N_0^m}\in\mathbb{R}^{N_0^m\times N_0^m}$ is an identity matrix, $\nu_r^m=\sqrt{Q_r^m/Q_r^{\text{master}}}$ is the mth substructure's scaling magnitudes which can be calculated; Q_r^{master} and $\lambda_r^{\text{master}}$ are the rth modal scaling factor and the rth system pole of master substructure respectively; the symbol "*" denotes complex conjugate. It is seen that the sign factors can be determined by minimizing the structure's potential energy from Equation (7).

Consider the higher modes have little influence on the potential energy and the minimum potential energy cannot guarantee the correctness of the automatic determination of the sign factors in higher modes. The orthogonality of mode shapes is used as constrained conditions of the optimization problem. Mode shapes have the following M-orthogonal: $\tilde{\psi}_r^T\mathbf{M}\tilde{\psi}_j\{\begin{matrix}\neq 0, r=j\\ =0, r\neq j\end{matrix}$, where $\mathbf{M}$ is the mass matrix. Assuming the mass distribution is uniform, it can be simplified as: $\tilde{\psi}_r^T\tilde{\psi}_j\{\begin{matrix}\neq 0, r=j\\ =0, r\neq j\end{matrix}$. The orthogonal angle between the vectors $\tilde{\psi}_r$ and $\tilde{\psi}_j$ is defined as

$$\theta_{rj}=\arccos\left(\frac{|\tilde{\psi}_r^{\mathrm{T}}\tilde{\psi}_j|}{\|\tilde{\psi}_r\|\,\|\tilde{\psi}_j\|}\right)(r\neq j) \tag{8}$$

where $\|\tilde{\psi}_r\|$ is the ℓ_2 norm of the vector $\tilde{\psi}_r$; the notation $|\cdot|$ represents the absolute value of variable. The orthogonal angle θ_{rj} can be used to measure the degree of orthogonality between two different assembled global mode shapes. Therefore, the following constraint conditions are designed for the optimization problem defined in Equation (7) to distinguish the feasible region from infeasible one,

$$\begin{aligned}\vartheta_r &= \min_{j\neq r}(\theta_{rj})\geq\vartheta_{\min}\\ \mu_r &= \tfrac{1}{N-1}\sum_{\substack{j=1\\ j\neq r}}^{N}\theta_{rj}\geq\mu_{\min}\\ \sigma_r &= \sqrt{\tfrac{1}{N-1}\sum_{\substack{j=1\\ j\neq r}}^{N}(\theta_{rj}-\mu_r)^2}\leq\sigma_{\max}\end{aligned} \tag{9}$$

where ϑ_r, μ_r, and σ_r are the minimum orthogonal angle, the mean value and the standard deviation of orthogonal angle for the rth mode, respectively. $\vartheta_{\min}$, $\mu_{\min}$, and $\sigma_{\max}$ are their corresponding threshold values provided in advance by expertise, and $\mu_{\min}$ should be slightly larger than $\vartheta_{\min}$. In this article, they are set to be 70°, 85°, and 10°, respectively. But how to use penalty techniques to transform the constraint conditions into an unconstrained optimization problem is still an essential issue to design a reasonable fitness function. This article proposes a fitness function to determine the sign factors by adopting penalty techniques.

According to the constraint conditions in Equation (9), define the following three penalty factors:

$$\begin{aligned}p_1 &= \sum_{r=1}^{N}\frac{[\sin(\vartheta_r)]^{\zeta_r}}{2^r}\\ p_2 &= \sum_{r=1}^{N}\frac{[\sin(\mu_r)]^{\zeta_r}}{2^r}\\ p_3 &= \sum_{r=1}^{N}\frac{[\cos(\sigma_r)]^{\zeta_r}}{2^r}\end{aligned} \tag{10}$$

where ζ_r is the factor to control the degree of punishment and it has the following values:

$$\zeta_r=\begin{cases}1\,(\vartheta_r\geq\vartheta_{\min},\mu_r\geq\mu_{\min},\sigma_r\leq\sigma_{\max})\\ \text{constant}>1\text{else}\end{cases} \tag{11}$$

It is obvious that the three penalty factors, p_1, p_2, and p_3 are less than 1. But for the points of the feasible region, their orthogonal angles will be approximately perpendicular; so the three penalty factors will be close to 1. In contrast, for the points of the infeasible region, their orthogonal angles will be far away from perpendicular; thus the three penalty factors will be correspondingly far away from 1. Through this strategy, the feasible and infeasible regions can be discriminated to some extent. Due to the value of potential energy $\pi_p(\eta_r)$ is usually a negative quantity and yet the fitness value should be better positive, the fitness function is defined as follows:

$$F(\eta_r)=-p_1p_2p_3\pi_p(\eta_r) \tag{12}$$

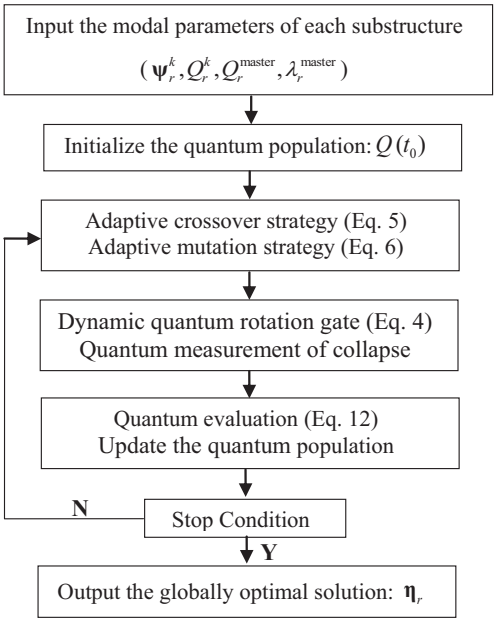

Fig. 5. Flowchart of the proposed optimization algorithm (QIGA).

2.4 The process of the QIGA-based optimization algorithm

As shown in Figure 5, the general framework of the proposed QIGA method is given. In the following, the basic steps of the proposed method are introduced.

Step 1. Input of the modal parameters of each substructure, such as the mode shape ψ_r^k and the modal scaling factor Q_r^k of the kth substructure, the modal scaling factor Q_r^{master} and the system poles $\lambda_r^{\text{master}}$ of the master substructure.

Step 2. Initialization of the quantum population, that is, an initial population of quantum individuals is randomly generated. Then, each individual is measured and the best candidate individual together with its fitness value is recorded for the use of iteration.

Step 3. Quantum population evolves. The adaptive crossover and mutation operators are conducted on the parent generation in turn to produce the offspring. It should be noted that the mutation operator is equivalent to implementing a quantum non-gate on a Q-bit.

Step 4. The dynamic quantum rotation gate is applied to the offspring of the quantum population. After that, a new quantum population is generated, and then each new individual is collapsed to a particular binary string by measurement. It should be noted that the binary string consists of two states, 1 and –1 instead of 1 and 0.

Step 5. These binary strings are evaluated by using the fitness function, meanwhile, replacing the old best candidate and its fitness value with the new ones according to the elitist strategy. Then, the parent generation is updated by replacing it with the new population generated from the operation of applied quantum rotation gate.

Step 6. Steps 4–6 are iteratively executed until the stop condition of the maximum generation set in advance reaches. Finally, the correct sign factors can be extracted from the best candidate of the last generation.

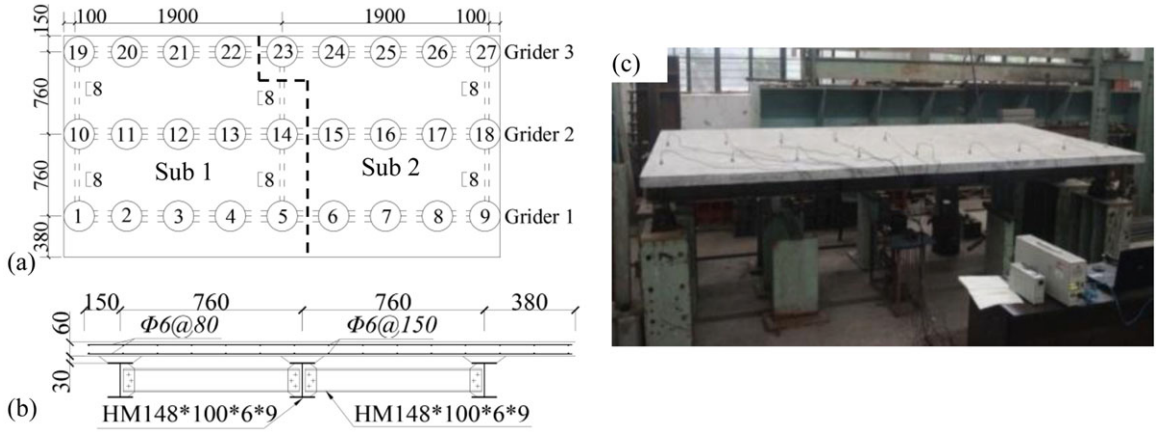

Fig. 6. Steel–concrete composite slab model: (a) dimension and instrumentation plan; (b) cross-section detail; and (c) photograph.

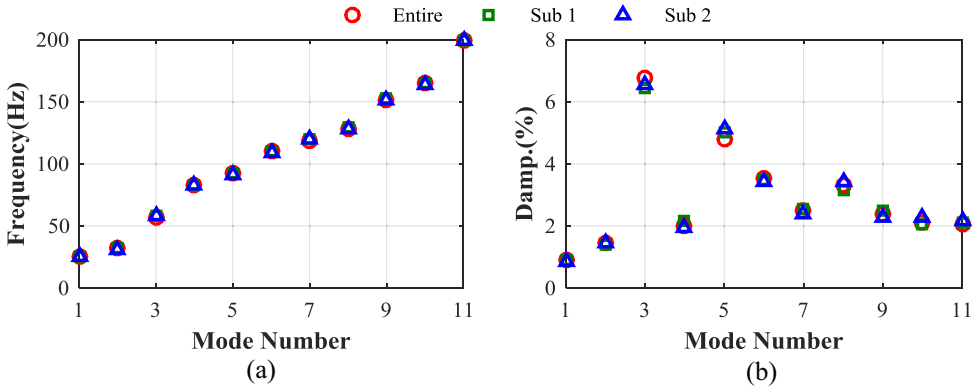

Fig. 7. Identified frequency and damping ratios.

Table 1
Magnitude adjustment factor and sign factor of the experimental example

Mode no.	v_r^2	η_r^2	*MAC*	*Mode no.*	v_r^2	η_r^2	*MAC*
1	0.84	1	0.9993	7	0.87	1	0.9934
2	1.13	1	0.9986	8	1.18	1	0.9992
3	−1.05	−1	0.9856	9	1.13	1	0.9993
4	0.96	1	0.9988	10	0.88	1	0.9957
5	−1.10	−1	0.9714	11	−0.91	−1	0.9878
6	−1.07	−1	0.9857	–	–	–	–

3 EXPERIMENTAL EXAMPLE OF A STEEL–CONCRETE COMPOSITE SLAB

To verify the effectiveness of the proposed method, the mobile impact test of a steel–concrete composite bridge model as shown in Figure 6 was performed. The model has an overall length of 4.0 m and a width of 2.05 m. Three I-shaped Q235 steel girders were constructed as longitudinal beams, connecting with concrete deck by cheese head studs. The structure was simply supported by three rolling supports (nodes 1, 10, 19) and three fixed supports (nodes 9, 18, 27). A PCB medium size impact hammer was used to impact the structure. Fifteen ICP accelerometers (0.5~7,000 Hz, acceleration $< 100\ g$) were mounted on the nodes of the slab, and a DP730 data acquisition system was used to acquire the impact test data.

As shown in Figure 6a, the steel–concrete composite bridge model was subdivided into two substructures. The hammer impact test was sequentially performed on substructures. Fourteen accelerometers were deployed on all nodes of Sub 1, and the impacting forces were applied to all nodes in turn except the rolling supporting nodes 1, 10, and 19. Sub 2 was tested by using thirteen accelerometers deployed on all nodes within this substructure and all nodes except the fixed supporting nodes 9, 18, and 27 were impacted. The technologies of bandwidth filtering and windowing in time domain were used to reduce noises and leakages of the collected impacting forces and accelerations. The CMIF method was employed to process the impact test data for structural modal parameter identification. The identified frequencies and damping ratios in the first eleven modes are shown in Figure 7.

Modal scaling factors, mode shapes and modal participation factors of the two substructures were identified. Choosing Sub 1 as the master substructure, for the first eleven modes identified, there are eleven

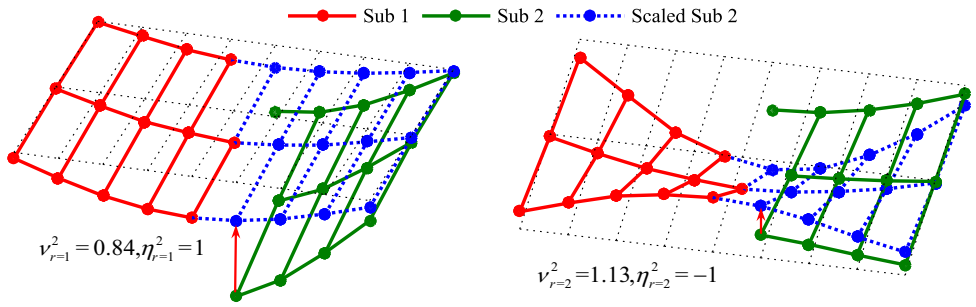

Fig. 8. The process of assembling mode shapes: (a) the first mode and (b) the second mode.

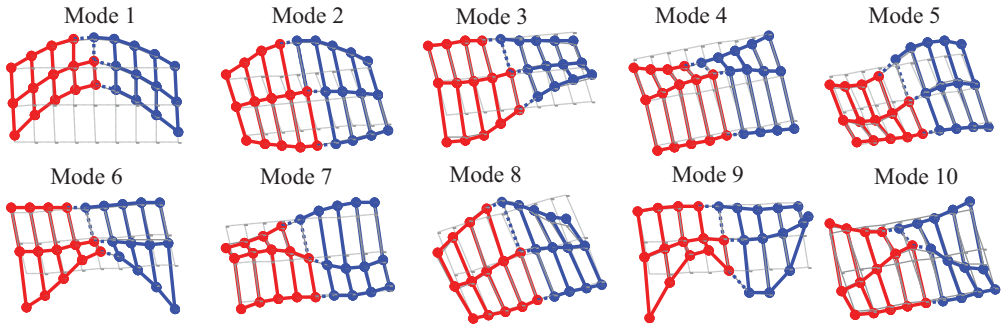

Fig. 9. The assembled global mode shapes of the ten modes.

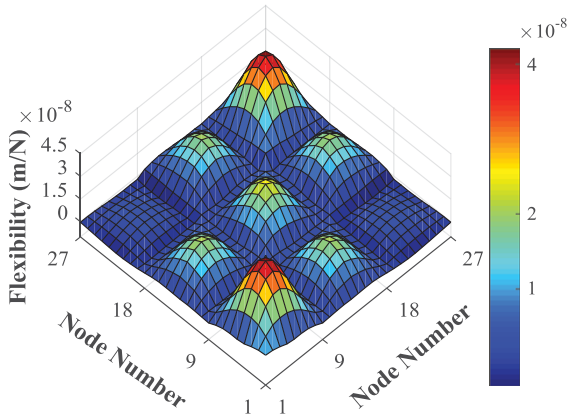

Fig. 10. The identified full modal flexibility matrix of the experimental example.

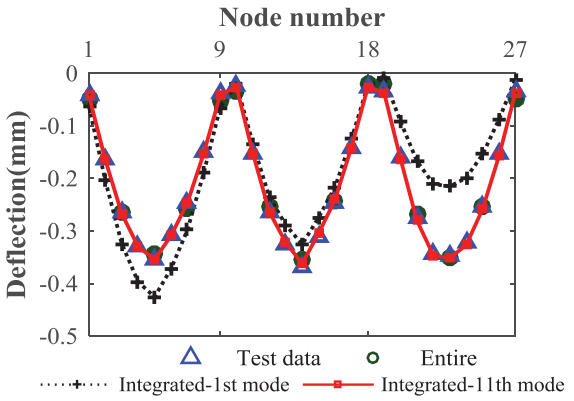

Fig. 11. The predicted defelction.

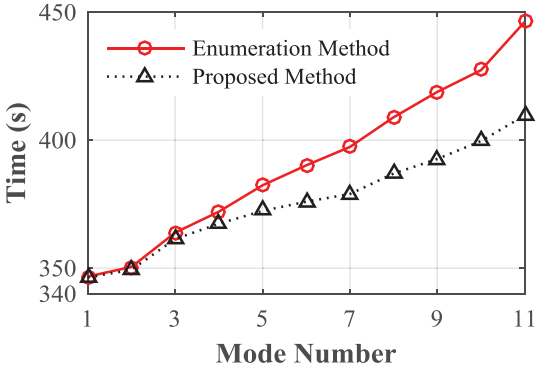

Fig. 12. The total time of the enumeration method and the proposed QIGA method.

sign factors needed to be determined. The magnitude adjustment factors and the sign factors of the eleven modes of Sub 2 are listed in Table 1. Modal Assurance Criterion (MAC) values calculated by the assembled global mode shapes and those from the traditional impact test method are also provided in Table 1. Figure 8 shows the process of assembling substructures' mode shapes of the first and the second mode. The assembled global mode shapes of the ten modes are shown in Figure 9.

The full modal flexibility matrix of the steel–concrete composite slab model was identified as shown in Figure 10. Figure 11 provides the predicted deflections from the identified flexibility when the uniform loads of 1.0 KN were applied to all nodes of the structure. The computational time of the enumeration method and the proposed QIGA method to solve the optimization problem are compared in Figure 12, which illustrates the high efficiency of the proposed QIGA method.

The performance of the QIGA is further compared with that of Quantum Genetic Algorithm (QGA) and GA to verify its effectiveness. In the comparison, 100 independent runs were executed for each algorithm. The probability of crossover and mutation were set to be 0.8 and 0.05 respectively in the GA method. The traditional constant quantum rotation angle strategy was used in the QGA method, in which the rotation angle is $\Delta\theta = 0.01\pi$. Figure 13 shows the evolving process of the three algorithms within 100 generations. The results of computations from the proposed QIGA, QGA, and GA

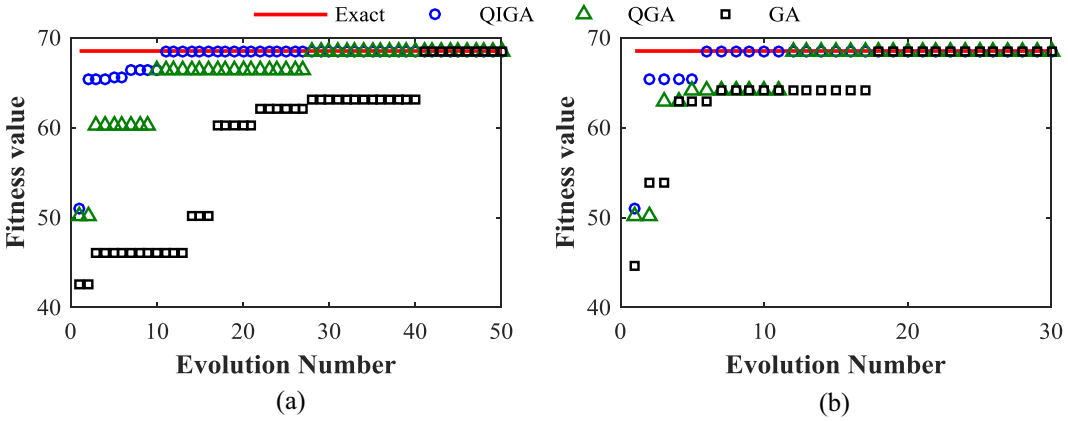

Fig. 13. Comparison of the maximum fitness values for the QIGA, QGA, and GA with: (a) population size of 10 and (b) population size of 50.

Table 2
Results comparison from the QIGA, QGA, and GA methods

			Fitness value				
Run times	*Test case*	*Algorithm*	*Best*	*Worst*	*Mean*	*Accuracy (%)*	*Evolution no.*
100	Case 1	GA	68.52	47.88	65.61	59	40
	10 individuals	QGA	68.52	68.52	68.52	100	28
	100 generations	QIGA	68.52	68.52	68.52	100	11
	Case 2	GA	68.52	68.52	68	97	18
	50 individuals	QGA	68.52	68.52	68.52	100	10
	100 generations	QIGA	68.52	68.52	68.52	100	5

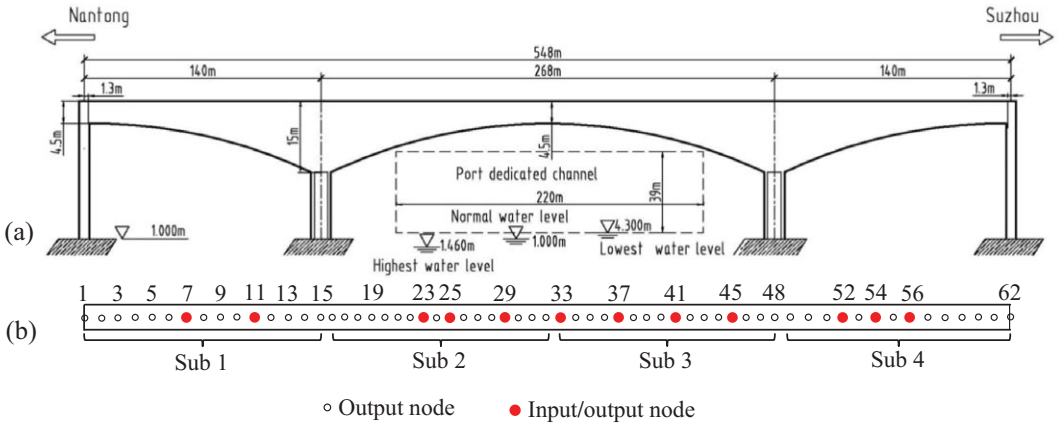

Fig. 14. The studied bridge (a) elevation view and (b) mobile impact test with reference-free measurement.

are shown in Table 2, in which the column of "Evolution no." denotes the average generation converging to the global optimum in the evolving process. It is clearly seen from Table 2 that the QIGA converges to the global optimum with a more fast speed than QGA and GA.

4 NUMERICAL EXAMPLE OF A THREE-SPAN CONTINUOUS RIGID-FRAME BRIDGE

The finite element model of a three-span continuous rigid-frame bridge (Figure 14) was studied to further verify the effectiveness of the proposed method. The

Table 3
Magnitude adjustment factor and sign factor of the numerical example

	The scaling factor			*The scaling factor sign*			
Mode no.	v_r^1	v_r^3	v_r^4	η_r^1	η_r^3	η_r^4	*MAC*
1	0.25	0.92	0.23	1	1	−1	0.9984
2	1.15	1.01	1.20	1	−1	1	0.9997
3	1.80	0.79	1.90	1	−1	−1	0.9991
4	0.69	1.03	0.72	−1	−1	−1	0.9996
5	0.33	0.85	0.31	−1	−1	−1	0.9980
6	1.40	1.04	1.41	1	1	1	0.9987
7	0.63	1.03	0.64	−1	1	−1	0.9995

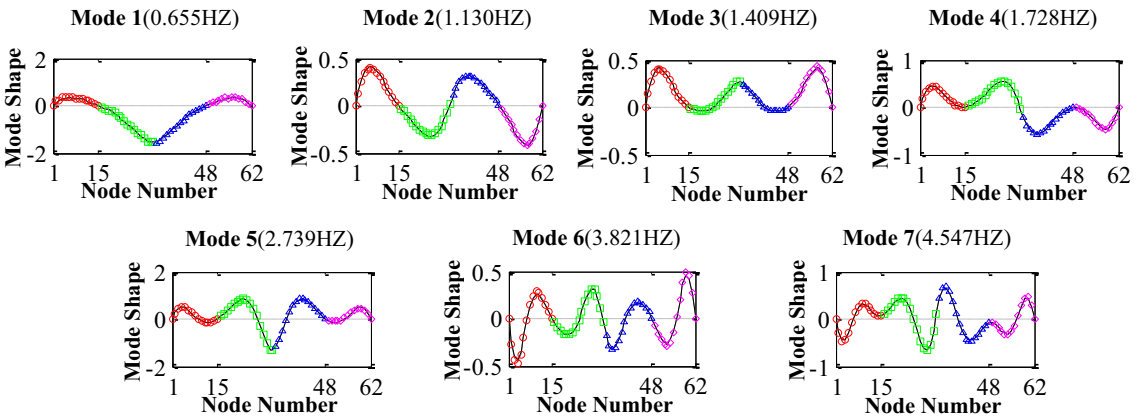

Fig. 15. Identified mode shape of the first seven modes.

bridge has an overall length of 548 m, with the length of the mid-span of 268 m and the length of two side spans of 140 m. The bridge deck is a two-way 6-lane road with a width of 34 m. The elasticity modulus, density, and Poisson ratio are 3.45E10 N/mm^2, 2,500 kg/m^3, and 0.2, respectively in this model. The finite element modeling of the bridge was constructed through the commercial ANSYS software.

The bridge was subdivided into four substructures as shown in Figure 14b, and the mobile impact test data were simulated through the dynamic analysis of the finite element model. Random white noise of 5% was added into the impacting forces and the accelerations to simulate observation noise. Because the node number of Sub 2 is larger than that of other substructures, it is chosen as the master substructure. The magnitude adjustment factors and the sign factors of Subs 1, 3, and 4 were calculated and their results are given in Table 3.

The assembled mode shapes of the structure of the first seven modes are shown in Figure 15. The full modal flexibility matrix of this structure was integrated as shown in Figure 16. To verify the accuracy of this flexibility matrix, applying a uniform load to the bridge in

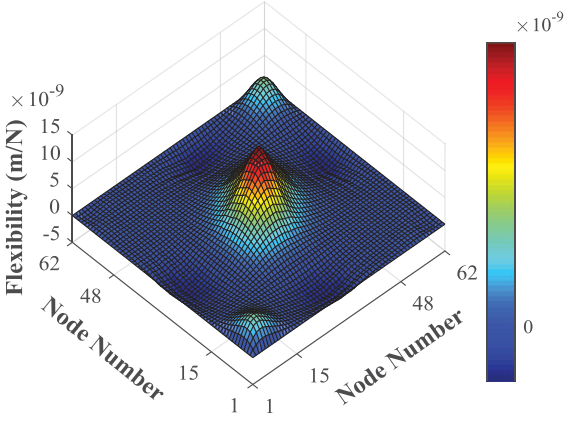

Fig. 16. The identified full modal flexibility matrix of the numerical example.

the form of every other node on the right-hand side of the bridge, this can lead to the prediction of the bridge's deflections by using the flexibility matrix as shown in Figure 17. It can draw the conclusion that only using modal parameters of lower orders cannot guarantee the

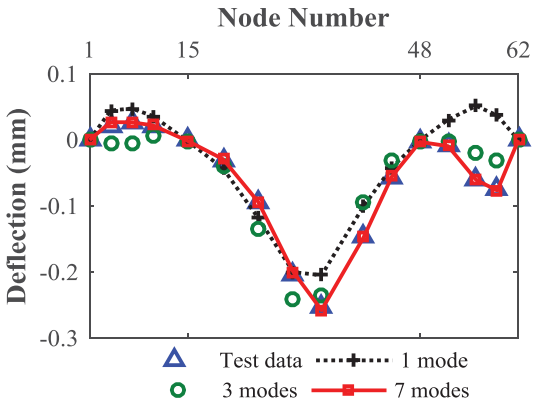

Fig. 17. The predicted deflections and the model truncation effects.

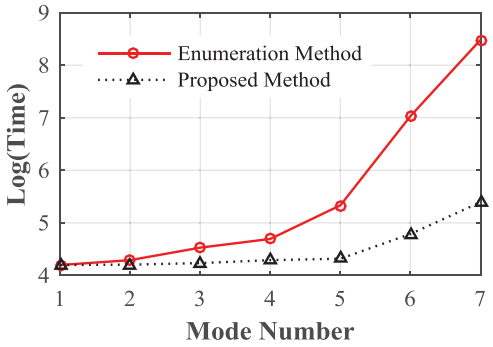

Fig. 18. The total time of the enumeration method and the proposed method.

accuracy of the integrated flexibility matrix, from the obvious difference between the deflections predicted using the modal parameters of the first three and the first seven orders.

Figure 18 shows the time cost of the enumeration method and the proposed QIGA method used for searching the twenty-first correct sign factors. It is seen that when the number of substructures becomes too large, the computational time of the enumeration method greatly increases with exponential rule, while the one of the QIGA method keeps relatively stable, which demonstrates the excellent efficiency of the QIGA method.

6 CONCLUSIONS

This article presents a new mobile impact testing method for structural flexibility identification, in which the key problem of determining the sign factor is transformed to a constrained optimization problem and it is solved by the developed QIGA method.

The QIGA has been improved by developing the adaptive crossover (mutation) strategy, dynamic quantum rotation gate. Compared to the traditional GA and QGA, the developed QIGA method can explore the search space with a smaller number of individuals and exploit the search space for a global solution within a short span of time, thus it is proved to be much more efficient for determining the sign factors.

An experimental example of a steel–concrete composite slab and numerical example of a three-span continuous rigid-frame bridge have been studied, and the results successfully verified the effectiveness of the proposed method by comparing with that of the traditional MRIT method for structural flexibility identification and deflection prediction. In addition, it should be noted that the proposed method is developed on the assumption that the structure has a uniform mass matrix. Whether it can be extended to inconsistent mass case will be studied in future work.

ACKNOWLEDGMENT

This work was sponsored by the National Natural Science Foundation of China (Grant No. 51108076).

REFERENCES

Amezquita-Sanchez, J. P. & Adeli, H. (2014), Signal processing techniques for vibration-based health monitoring of smart structures, *Archives of Computational Methods in Engineering*, **23**(1), 1–15.

Beg, A. H. & Islam, M. Z. (2016), Novel crossover and mutation operation in genetic algorithm for clustering, in *Proceedings of the IEEE Congress on Evolutionary Computation*, IEEE, 2114–21.

Brown, D. L. & Witter, M. C. (2011), Review of recent developments in multiple reference impact testing (MRIT), *Structural Dynamics*, **45**(1), 8–17.

Brownjohn, J. M., Magalhaes, F., Caetano, E. & Cunha, A. (2010), Ambient vibration re-testing and operational modal analysis of the Humber Bridge, *Engineering Structures*, **32**(8), 2003–18.

Catbas, F. N., Brown, D. L. & Aktan, A. E. (2004), Parameter estimation for multiple-input multiple-output modal analysis of large structures, *Journal of Engineering M—ASCE*, **130**(8), 921–30.

Catbas, F. N., Kijewski-Correa, T. & Aktan, A. E. (eds.). (2013), *Structural Identification of Constructed Systems: Approaches, Methods, and Technologies for Effective Practice of St-Id*, ASCE, Reston, VA.

Cha, Y. & Buyukozturk, O. (2015), Structural damage detection using modal strain energy and hybrid multiobjective optimization, *Computer-Aided Civil and Infrastructure Engineering*, **30**(5), 347–58.

De Vitis, J., Masceri, D., Aktan, A. E., and Moon, F. L. (2013), Rapid structural identification methods for

high-way bridges: towards a greater understanding of large populations, in *Proceedings of the 11th International Conference on Structural Safety & Reliability*, Columbia University, NY, USA.

Guo, S., Zhang, X., Zhang, J., Zhou, Y., Moon, F. & Aktan, A. E. (2018), Mobile impact testing of a simply-supported steel stringer bridge with reference-free measurement, *Engineering Structures*, **159**, 66–74.

Han, K. & Kim, J. (2000), Genetic quantum algorithm and its application to combinatorial optimization problem, in *Proceedings of the Congress on Evolutionary Computation*, IEEE, 1354–60.

He, X., Moaveni, B., Conte, J. P., Elgamal, A. & Masri, S. F. (2008), Modal identification study of VincentThomas Bridge using simulated wind-induced ambient vibration data, *Computer-Aided Civil and Infrastructure Engineering*, **23**(5), 373–88.

Jiang, X. & Adeli, H. (2008), Neuro-genetic algorithm for nonlinear active control of highrise structures, *International Journal for Numerical Methods in Engineering*, **75**, 770–86.

Kociecki, M. & Adeli, H. (2014), Two-phase genetic algorithm for topology optimization of free-form steel space-frame roof structures with complex curvatures, *Engineering Applications of Artificial Intelligence*, **32**, 218–27.

Li, H., Ou, J., Zhao, X., Zhou, W., Li, H., Zhou, Z. & Yang, Y. (2006), Structural health monitoring system for the Shandong Binzhou Yellow River highway bridge, *Computer-Aided Civil and Infrastructure Engineering*, **21**(4), 306–17.

Lynch, J. P. (2002), Decentralization of wireless monitoring and control technologies for smart civil structures. Ph.D. dissertation of Civil and Environmental Engineering, Stanford University, CA, USA.

Marulanda, J., Caicedo, J. M. & Thomson, P. (2016), Modal identification using mobile sensors under ambient excitation, *Journal of Computing in Civil Engineering*, **31**(2), 04016051.

Mencia, R., Sierra, M. R., Mencia, C. & Varela, R. (2016), Genetic algorithms for the scheduling problem with arbitrary precedence relations and skilled operators, *Integrated Computer-Aided Engineering*, **23**(3), 269–85.

Putha, R., Quadrifoglio, L. & Zechman, E. M. (2012), Comparing ant colony optimization and genetic algorithm approaches for solving traffic signal coordination under oversaturation conditions, *Computer-Aided Civil and Infrastructure Engineering*, **27**(1), 14–28.

Sadhu, A., Narasimhan, S. & Goldack, A. (2014), Decentralized modal identification of a pony truss pedestrian bridge using wireless sensors, *Journal of Bridge Engineering*, **19**(6), 04014013.

Sgambi, L., Gkoumas, K. & Bontempi, F. (2012), Genetic algorithms for the dependability assurance in the design of a long-span suspension bridge, *Computer-Aided Civil and Infrastructure Engineering*, **27**(9), 655–75.

Shabbir, F. & Omenzetter, P. (2015), Particle swarm optimization with sequential niche technique for dynamic finite element model updating, *Computer-Aided Civil and Infrastructure Engineering*, **30**(5), 359–75.

Zhang, J., Guo, S. & Chen, X. S. (2014), Theory of un-scaled flexibility identification from output-only data, *Mechanical Systems and Signal Processing*, **48**(1), 232–46.

Zhang, J., Guo, S. L. & Zhang, Q. Q. (2015), Mobile impact testing for structural flexibility identification with only a single reference, *Computer-Aided Civil and Infrastructure Engineering*, **30**(9), 703–14.

Zhang, J., Prader, J., Grimmelsman, K. A., Moon, F., Aktan, A. E. & Shama, A. (2013a), Experimental vibration analysis for structural identification of a long-span suspension bridge, *Journal of Engineering Mechanics—ASCE*, **139**(6), 748–59.

Zhang, J., Wan, C. & Sato, T. (2013b), Advanced Markov Chain Monte Carlo approach for finite element calibration under uncertainty, *Computer-Aided Civil and Infrastructure Engineering*, **28**(7), 522–30.